Received: 8 July 2021 | Revised: 27 October 2021 | Accepted: 22 November 2021

DOI: 10.1049/hve2.12180

High Voltage

ORIGINAL RESEARCH

Characteristics of pantograph-catenary arc under low air pressure and strong airflow

Zhilei Xu[1] | Guoqiang Gao[1] | Wenfu Wei[1] | Zefeng Yang[1,2] | Wenhan Xie[1] | Keliang Dong[1] | Yaguang Ma[1] | Yan Yang[1,3] | Guangning Wu[1]

[1]School of Electrical Engineering, Southwest Jiaotong University, Chengdu, China

[2]Department of Research and Development, Chengdu Guojia Electrical Engineering Co. Ltd, Chengdu, China

[3]School of Electrical & Electronic Engineering, Nanyang Technological University, Singapore, Singapore

Correspondence

Wenfu Wei, School of Electrical Engineering, Southwest Jiaotong University, 610031, Chengdu, China.
Email: wfwei@home.swjtu.edu.cn

Associate Editor: Dunpin Hong.

Funding information

NEEC project, Grant/Award Number: NEEC-2018-B06; National Natural Science Foundation of China, Grant/Award Numbers: 51807167, 51837009, 51922090, 52077182, U19A20105; Science and Technology Project of Headquarter of SGCC, Grant/Award Number: SGTYHT/19-JS-215

Abstract

Pantograph-catenary arc fault is the primary factor threatening the stability of the power transmission for high-speed railway. The motion characteristics of the pantograph-catenary arc under low air pressure and strong airflow is significantly different from the case under atmospheric pressure. In this paper, an experimental platform of pantograph-catenary arc was built to investigate arc root position-time and arc column longitudinal drift height-time characteristic curves under different air pressures and airflow velocites. Via analysing the corresponding results, it can be found that there are different arc root–arc column traction mechanisms at different stages of arc development. The arcing time and arc root stagnation time under low air pressure are significantly longer than the case under atmospheric pressure, resulting in more serious electrode ablation. The arc column longitudinal drift velocity and height are greater with the increase of airflow velocity. Two typical irregular arc motion phenomena—arc root jumping and arc reignition are observed. To clarify the internal mechanism of the above phenomenon, a magnetohydrodynamics (MHD) model of the pantograph-catenary arc was lauched, the influence mechanism of the pantograph-catenary arc temperature and voltage are studied, and the physical process of arc temperature oscillation is analysed. The research results provide theoretical support for arc protection in high-altitude areas.

1 | INTRODUCTION

As a critical power transmission intermedia, the carbon-copper electrode pairs have high electrical conductivity, impact resistance, excellent self-lubricating properties, etc. As sliding electrical contact materials, they are widely applied in the pantograph-catenary systems, grounding brushes, collector rings, and so on for high-speed railway [1–5]. The pantograph-catenary system plays a key role in the enery supply for high-speed trains. During the dynamic process of high-speed trains, the carbon-copper electrode of the pantograph-catenary system is subjected to vibration impact and rigid-point impact, which breaks the contact state of the electrodes frequently. As the arc occurs frequently, the interaction between the electrode and the arc ablates the electrode seriously. According to statistics, the fault caused by the pantograph-catenary arc has become the primary factor threatening the power supply safety of high-speed railways, and caused serious losses [6–9]. For high-speed trains operate under low air pressure and strong airflow, in the developing Sichuan–Tibet Railway in China for example, the frequency of arc occurrence will be higher, and the arc ablation will be more serious. Moreover, the longitudinal drift of the arc column will cause the arc to develop to the bus bar, which may lead to the flashover of the supporting insulator [10]. However, the characteristics and influencing factors of the arc root motion, arc root jumping, arc root

stagnation, and arc column longitudinal drift characteristics in low air pressure and strong airflow are still unclear. Therefore, it is of great significance to investigate the motion characteristics of the pantograph-catenary arc under strong airflow condition with low air pressure to reduce arc appearence and consequent erosion.

So far domestic and foreign scholars' research on the development and movement characteristics of the arc under atmospheric pressure mainly focusses on switching electric arc and low-voltage circuit breaker arc [11–15], and the main characteristics are obtained. Meanwhile the research on the arc movement characteristics under low air pressure mainly focusses on the arc of vacuum circuit breaker and the arc under extremely low air pressure (<0.3 atm) environment [16–19]; the characteristics of arc movement in a vacuum environment, and extremely low air pressure are explained. Although the above-mentioned research on arc movement characteristics in low air pressure environments is carried out in extremely low air pressure (<0.3 atm) environments for switching gears, it is still unclear if there is difference in the arc movement characteristics in low air pressure environments (0.5–1 atm). Plus, the switching electrical arc is in a closed container, and the arc is thermally insulated from the outside, but the pantograph-catenary arc is completely exposed to the strong airflow formed by the high-speed travelling wind, and the two electrodes of the pantograph-catenary arc are in the state of high-speed tangential sliding and normal vibration. It is safe to say the development of the arc motion is completely different from the switching electrical arc.

The research on the influence of airflow velocity on arc motion characteristics mainly focusses on the UHV secondary arc and partial arc of high-altitude DC insulators [20–22]. The influence of different airflow velocitied on motion characteristics of UHV secondary arc is focused in [20, 21]; however, it considers that the airflow velocity (about 5 m/s) is very different from the airflow velocity of the pantograph arc (about 30 m/s), and the arc motion characteristics and influence mechanism are significantly different from those under low air pressure and strong airflow. Zhang et al. [22] established a chain model for the partial arc of high-altitude DC insulators and studied the arc drift characteristics under multi-field stress. However, the arc current of the pantograph-catenary is about 10^7 times that of the partial arc current of the insulator, so the motion characteristics of the arc are also quite different from that of the pantograph-catenary arc. In terms of pantograph-catenary arc motion characteristics, the related studies mainly focus on arc motion characteristics and electrode ablation in the process of lowering the pantograph under atmospheric pressure [23–29]. However, the arc root motion characteristics, arc column longitudinal drift characteristics, and their influencing mechanism have not been studied in low air pressure (0.5–1 atm) and strong airflow.

In this paper, the experimental platform of the pantograph-catenary arc under strong airflow condition with low air pressure is built in this study, meanwhile the arc root position-time and arc column longitudinal drift height-time characteristic curves under different air pressure and airflow velocities were established to explore the characteristics of arc motion. The phenomenon of arc root jump and arc reignition and its influence mechanism under low air pressure are analysed. A magnetohydrodynamics (MHD) model was established to analyse the influence of different air pressures and airflow velocities on the temperature and voltage of the pantograph-catenary arc. The research results provide theoretical support for reducing pantograph-catenary arc faults and realizing arc control under low air pressure.

2 | THE PHENOMENON OF ARC ROOT JUMPING AND ARC REIGNITION UNDER LOW AIR PRESSURE AND STRONG AIRFLOW

2.1 | Experiment platform and test method

An experiment platform of pantograph-catenary arc under strong airflow condition with low air pressure was built. The main experimental devices include a power supply, low air pressure tank, arc generator, high-speed camera, oscilloscope, and a current limiting resistor as shown in Figure 1a. The arc generator is composed of the copper–carbon electrode, displacement controller, and precision displacement stage controlled by the stepping motor;

The power supply is a constant current DC power supply, and the output current is 0–150 A, which is consistent with the traction current through a single pantograph when a high-speed train is running. At the beginning of the experiment, the copper electrode and the carbon electrode were fixed on the precision table. Meanwhile, the carbon-copper electrodes were in contact with each other at a distance of 0 mm. Then, the precision displacement table was operated to separate the carbon and copper electrodes, thus, the pantograph-catenary arc is produced. A Hall current sensor (WHK LB5S2) and an active voltage probe (Tektronix TAP0250) were used to record the arc current, and a digital oscilloscope (Tektronix MDO3024, bandwidth frequency of 200 MHz) was used to record the voltage waveform. The current came from the constant current DC source, passing through a current limiting resistor, copper–carbon electrode pairs, and finally back to the power supply. A high-speed camera (FASTCAM Nova S6) is used to capture the arc motion process. A stepless speed regulating fan was used in the experiment, and the wind speed could continuously be adjustable from 0 to 60 m/s. The fan outlet is fixed 10 cm away from the electrode, and the central axis of the fan outlet is parallel to the contact point of the carbon-copper electrode to ensure that the fan airflow is parallel to the electrode streamline. During the experiment, the switch of the fan was adjusted to control the wind speed, and the precision anemometer was used to measure the wind speed at the electrode. The average value was repeated five times to eliminate the error to determine the wind speed at the electrodeposition of 10, 20, and 30 m/s, respectively.

Figure 1b shows the schematic diagram of the arc root position and the arc column longitudinal drift height, defining

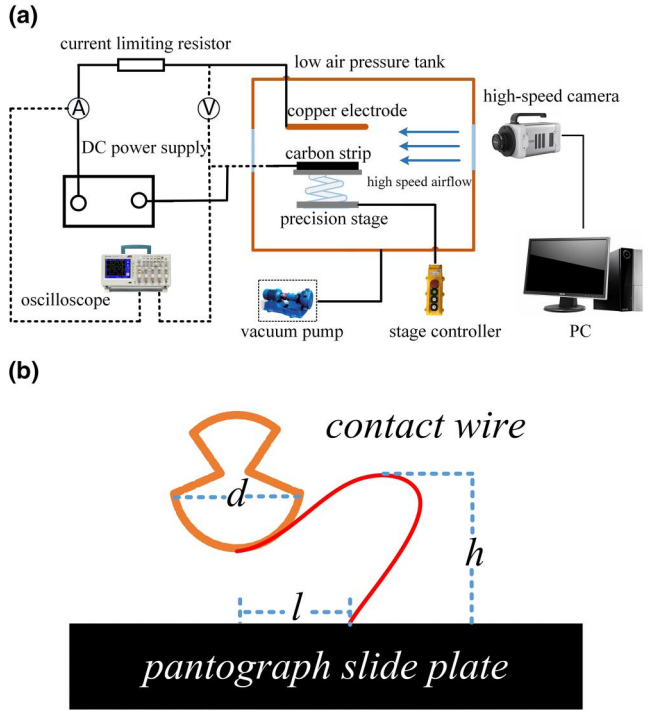

FIGURE 1 The pantograph-catenary arc experiment platform and test method under low air pressure (a) The pantograph-catenary arc test and diagnosis platform (b) Schematic diagram of the arc root position and the arc column longitudinal drift height

the arc column longitudinal drift height as the distance between the highest point of the arc column and the upper surface of the carbon slide plate. In Figure 1b, l, h, and d are the arc root position, arc column longitudinal drift height, and contact line diameter measured from the arc image at time t_1, respectively; selecting the actual diameter d_1 of the contact line as the reference; then the actual arc root displacement l_1 and arc column longitudinal drift height h_1 at time t_1 are

$$l_1 = \frac{d_1 l}{d} \tag{1}$$

$$h_1 = \frac{d_1 h}{d} \tag{2}$$

In the same way, the arc root displacement l_2 and the arc column longitudinal height h_2 at t_2 can be calculated according to the arc image; then the arc root movement velocity v_1 and the arc column longitudinal drift velocity v_2 can be calculated as follows:

$$v_1 = \frac{l_2 - l_1}{t_2 - t_1} \tag{3}$$

$$v_2 = \frac{h_2 - h_1}{t_2 - t_1} \tag{4}$$

2.2 | Development process of the pantograph-catenary arc

A high-speed camera is used to photograph the development process of pantograph-catenary arc movement when the air pressure is 60 kPa and the airflow velocity is 20 and 30 m/s, respectively, as shown in Figure 2a. It can be found that with the increase of airflow velocity, the arc develops faster, and the arc column longitudinal drift is more intense.

It is worth noting that the airflow velocity has a great influence on the migration of the arc root, and the arc root movement speed under low airflow velocity is lagging. For example, when the airflow velocity is 30 m/s, the arc root moves to 16.01 mm away from the copper electrode in 5 ms, and the moving distance of the arc root is 1.68 times of that when the airflow velocity is 20 m/s.

Figure 2b shows the arc voltage and current waveform when $P = 60$ kPa and $V = 30$ m/s. In the initial stage of arc burning, the arc voltage is relatively stable with a small amplitude change. When the arc develops to about 50 ms, the arc voltage increases gradually and the voltage fluctuation is obvious. At the end of arc burning, the arc oscillates frequently, and the arc stability is poor.

Via analysing the voltage and current waveforms, it is found that the waveform mutation occurs in the late stage of arc burning. Combined with the analysis of arc burning images, it is found that arc reignition occurs at the waveform mutation. It can be seen from Figure 2b that when the arc is extinguished, the voltage between the electrodes is restored to the power supply voltage, meanwhile, the arc voltage curve rises sharply. When the arc is reignited, the arc voltage curve drops sharply and the voltage between the electrodes becomes the arc voltage. Thus, an oscillation process on the voltage waveform represents an arc reignition process.

2.3 | The influence mechanism of arc root jumping under low air pressure

To explore the arc root jumping phenomenon of the pantograph-catenary arc under low air pressure and strong airflow found in the experiment, combined with the arc development process, the arc root motion characteristic curve at $P = 60$ kPa and $V = 20$ m/s is analysed. A descending-stagnating-rising period of the arc root curve was a complete arc root jump process as shown in Figure 3. At $t = 181.64$ ms, the arc root is at point B, which is 10.5 mm from the contact line. When the arc develops to $t = 186.32$ ms, the arc column has an air breakdown with the anode at point A, which is 5.1 mm from the contact line. At this time, a bright spot can be seen at point A. Until $t = 191$ ms, it is completely broken down and a new arc root is formed. At this time, two arc roots coexist for a short time. Because the original arc root resistance is relatively large and the current is relatively small, it is not enough to maintain a stable arc. Therefore, when the arc develops to $t = 200.36$ ms, the original arc root is gradually extinguished and finally replaced by the new arc root. At this point, the arc root jump is completed.

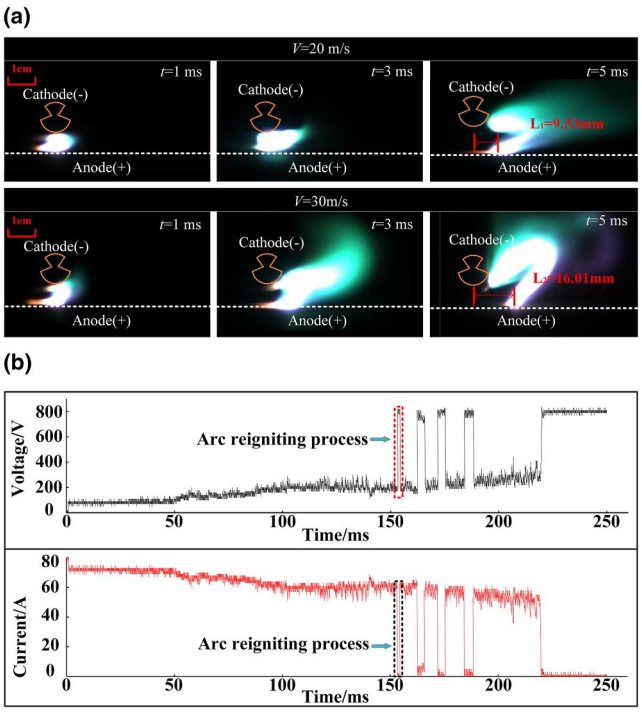

FIGURE 2 Experimental arc burning image and the arc voltage and current waveform. (a) Arc development process under different airflow velocities at p = 60 kPa, (b) Arc voltage and current waveform when p = 60 kPa and V = 30 m/s

2.4 | Arc reignition characteristics under the combined action of low air pressure and strong airflow

The high-speed camera is used to capture images of the arc reignition process when the arc develops to around t = 160 ms under the condition of P = 60 kPa and V = 30 m/s as shown in Figure 4. Via analysing the corresponding results, it can be found that at t = 150 ms, the arc column is stretched violently and the longitudinal drift under the combined action of the transverse wind load and the vertical upward thermal buoyancy, the arc length reaches the maximum value before extinguishing. The stretching and longitudinal drift of the arc column aggravate the heat loss, and the recombination and diffusion of electrons and positive ions are enhanced, which accelerates the de-ionization process of the arc. The temperature of the arc column gradually decreases and the arc begins to extinguish. When the arc develops to t = 156.9 ms, the arc is completely extinguished. However, it can be observed that the cathode and anode have a "bright spot" respectively. At this time, the air insulation strength has not yet fully recovered. At t = 159.2 ms, it can be seen that the "purple arc" starts to develop from the arc root to the cathode arc root until it is completely broken down and the arc reignites. After the arc reignites, it develops rapidly. When the arc develops to t = 161.5 ms, it starts to burn violently and quickly returns to the state before extinguishing.

It can be found that arc reignitions are more frequent under low air pressure and strong airflow. There are two possible reasons for this phenomenon: on the one hand, the strong airflow makes the arc column stretch seriously, and the arc heat loss is aggravated, which speeds up the arc de-ionization; the convection heat dissipation between the pantograph-catenary arc and the surrounding air is accelerated under the action of strong airflow, leading to decrease in the arc temperature, and also promotes the de-ionization process of the arc, making it easier to extinguish. On the other hand, the air breakdown voltage is lowered under low air pressure, and after the arc is extinguished, it is easier to break down again in the original arc channel, causing the arc to reignite.

3 | MOTION CHARACTERISTICS OF THE PANTOGRAPH CATENARY ARC UNDER LOW AIR PRESSURE AND STRONG AIRFLOW

3.1 | Arc root motion characteristics under different air pressures and airflow velocities

The air pressure has a significant influence on the arc movement as shown in Figure 5a. The arc root motion at different airflow velocities can be divided into the initial stage, the rapid development stage, and the terminal frequent jumping stage. In the initial stage of the arc, the electromagnetic force plays a major role in the arc movement; however, the electromagnetic force at the arc root is relatively large [20, 21], and the movement velocity of the arc root is greater than that of the arc column, meanwhile, the traction mechanism of pantograph-catenary arc movement is shown as arc root traction arc column movement. With the development of the arc, the wind on the arc column begins to play a leading role. At this time, the traction mechanism of arc movement is shown as arc column traction arc root movement, and the arc root movement velocity exceeds any time before; the greater the airflow velocity, the greater the arc root motion acceleration. In the later stage of arc development, the arc root-time curve has frequent periodic oscillation. The arc root moves slower under low air pressure than that under atmospheric pressure. This is because the diameter of the arc column becomes larger under low air pressure. As the air pressure decreases, the dynamic viscosity of the air decreases, resulting in a decrease in the arc root movement speed under the traction of the arc column. In addition, the arc root jumping frequency varies greatly under different air pressures. When the air pressure is 60, 80, and 101 kPa, the number of arc root jumping is 5.2 times, 2.9 times, and 1.8 times, respectively. It shows that the arc stability under low air pressure is worse.

It can be seen from Figure 5b that the average oscillation frequency is 1.9, 3.1, and 4.2 at the airflow velocity of 10, 20, and 30 m/s, and the oscillation frequency at 30 m/s is higher than that of the lower airflow velocity; this is because an

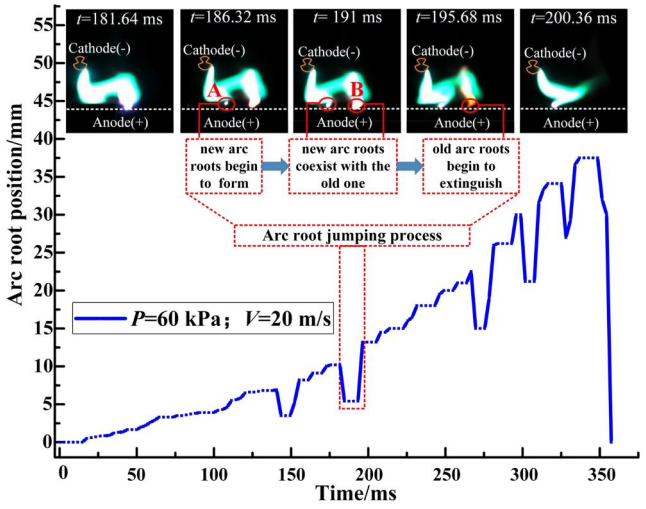

FIGURE 3 Arc root jumping under low air pressure

oscillation period represents a complete process of the arc root jump. In the later stage of arc development, the stability of the arc decreases, and the arc root jumps more frequently.

The arc jumping frequency is higher under low air pressure and strong airflow. There are two possible reasons for this result: on the one hand, the arc column approaches the anode, the temperature of the air near the anode rises rapidly, the air insulation strength is weakened, and air breakdown is more likely to occur. On the other hand, the air breakdown voltage threshold is lowered under low air pressure, so that the arc column and the anode pole's uneven electric field are broken down, forming a new arc root. Therefore, the arc root jumps more frequently under low air pressure.

It is worth noting that with the decrease of air pressure, the stagnation time of arc roots increases significantly. The total stagnation time of arc roots when the air pressure is 60, 80, and 101 kPa are 145.31, 93.75, and 65.63 ms, respectively. Long-term residence of the arc root causes severe ablation of the electrode. In addition, the arcing time is longer under low air pressure, which exacerbates the ablation of the electrode.

3.2 | Motion characteristics of arc column under different air pressures and airflow velocities

To further investigate the influence of air pressure and airflow velocity on the movement of the arc column, the arc column longitudinal drift height-time characteristic curve under different air pressures and airflow velocities is established to characterise the arc longitudinal motion characteristics. Figure 6 shows the changing law of the arc column longitudinal drift height-time curve under different air pressures and airflow velocities. Figure 6a shows the change of the arc column longitudinal drift height in the whole process of arc development under different airflows at $P = 60$ kPa. In the early stage of arc development, the arc column moves under the traction of the arc root, meanwhile the wind load and thermal buoyancy are small, and the horizontal stretching and longitudinal drift of the arc column are slow. At this time, the airflow velocity has almost no effect on the arc column longitudinal drift height. In the middle stage of arcing, the arc begins to develop rapidly, and the faster the airflow velocity, the greater the arc longitudinal drift velocity. For example, when the air velocity is 10, 20 and 30 m/s, the arc column longitudinal drift velocity is 1.69, 2.13 and 3.35 m/s, respectively. The above phenomenon is caused by the rapid stretching and bending of the arc column due to the blowing of the airflow; the wind load and thermal buoyancy of the arc column increased rapidly, and the arc column moved faster in the transverse and longitudinal direction, which also proved that the traction mechanism of the arc root–arc column changed at this time.

It is found from the analysis of Figure 6b that the arc column longitudinal drift height is higher under low air pressure. In the early stage of arc development, the arc height increases slowly, and there is no difference in the longitudinal arc drift velocity and height of the arc column under different air pressure levels. In the middle and late stages of arc development, the influence of air pressure on the arc column longitudinal drift height is more obvious, and the longitudinal arc drift degree of the arc column is more serious under low air pressure. Therefore, it is easier for the arc to float to the rigid catenary bus bar under low air pressure, causing the flashover of the supporting insulator string.

It was found that the frequent oscillation of the arc height-time characteristic curve is in the later stage of arc development under low air pressure and strong airflow. The arc column longitudinal drift height dropped from the peak to zero in an instant and then quickly recovered to the peak. Combined with the arc development image, it can be seen that an oscillation period indicates the process of arc extinguishment and reignition. Under the same experimental conditions, the experiment was repeated 5 times and the average value was calculated: when $P = 60$ kPa, and $V = 10$, 20 and 30 m/s, and the arc reignition frequency was 0, 3.1, and 4.2, respectively. When $V = 20$ m/s, and $P = 60$, 80, and 101 kPa, the arc reignition times are 3.2, 1.8 and 0, respectively. This shows that the arc reignition frequency is higher under low air pressure and strong airflow, and the arc is more difficult to extinguish, with the electrode ablation being more serious.

4 | MHD MODEL OF THE PANTOGRAPH-CATENARY ARC UNDER LOW AIR PRESSURE AND STRONG AIRFLOW

4.1 | Geometric model and material parameters

In this paper, a geometric model of the pantograph-catenary system under low air pressure and strong airflow is established, as shown in Figure 7. The calculation area includes air domain, contact wire, and pantograph slide strip. The contact wire material and radius used in the model are consistent with the actual

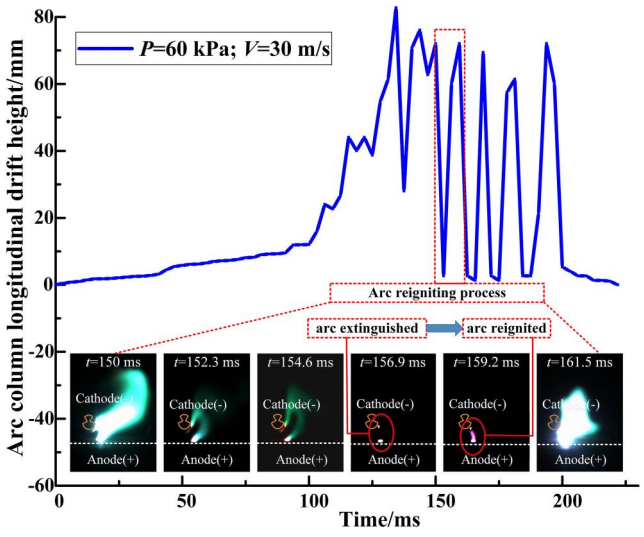

FIGURE 4 Arc reignition under low air pressure and strong airflow

wire parameters. The bottom contour radius of the contact wire is 6.5 mm. The length of the carbon slide strip is 150 mm and the thickness is 20 mm. The initial length of the pantograph-catenary arc is set to 4 mm [30]. Table 1 lists the specific parameter settings of the pantograph and catenary materials in the model.

4.2 | Physical model and the governing equation

The development process of arc plasma involves the multi-field coupling of the electric field, magnetic field, thermal field, force field, and airflow field. Its physical parameters include thermal conductivity, temperature, specific heat capacity, pressure, and electrical conductivity. In the simulation calculation process, the following basic assumptions are used to simplify the simulation of arc plasma:

(1) At the beginning of the simulation, the pantograph-catenary arc plasma has steadily existed between the contact line and the pantograph slide plate and is in a state of local thermodynamic equilibrium (LTE);
(2) The plasma is electrically neutral and there is no space charge;
(3) The phase transition between the contact line and the pantograph slide plate and the composition of copper vapour and carbon vapour produced by it are not considered;
(4) The flow property of pantograph-catenary arc plasma is laminar flow;

The governing equations of the physical model described before [30, 31], include mass conservation equations, energy conservation equations, momentum conservation equations, and electromagnetic field equations. The governing equations are as follows:

(1) Mass conservation equations:

$$\frac{\partial \rho}{\partial t} + \nabla \cdot (\rho \mu) = 0 \tag{5}$$

ρ is the arc density; t is the time; μ is the fluid movement speed.

(2) Energy conservation equations:

$$\frac{\partial (\rho T)}{\partial t} + \nabla \cdot (\rho v_f T) = div\left(\frac{\lambda}{c_p} \nabla T\right) + S_T \tag{6}$$

S_T is the source term of the energy conservation equation, which can be expressed as:

$$S_T = V_w + \frac{J^2}{\sigma} - Q_R \tag{7}$$

T is the temperature; v_f, c_p and λ are the fluid velocity, specific heat capacity, and thermal conductivity, respectively, which depend on temperature and pressure and are taken from literature [32]; V_w is the fluid viscous dissipation terms; J and σ are the current density and electrical conductivity of the arc plasma, respectively. Q_R is the arc radiation energy source term through thermal radiation [30]. In the simulation model, the volume net emissivity is used to characterise the arc radiation energy dissipation, and Q_R can be expressed as follows:

$$Q_R = 4\pi \varepsilon_R \tag{8}$$

ε_R is the volumetric net emissivity [31, 33, 34]

(3) Momentum conservation equations:

The solution of the velocity field in the momentum conservation equation in the model is described by Navier–Stokes equations [35], and its expression is

$$\frac{\partial (\rho v_i)}{\partial t} + \nabla \cdot (\rho v_i u) = \nabla \cdot (\eta \nabla v_i) - \frac{\partial p}{\partial x_i} + S_{v_i} \tag{9}$$

S_{vi} is the source term of the momentum conservation equation, which can be expressed as

$$S_{v_i} = (J \times B)_i + \rho g \tag{10}$$

v_i is the velocity component in the $i(i = \mathrm{x}, \mathrm{y})$ direction, η、p、J and B are the dynamic viscosity coefficient, pressure, arc

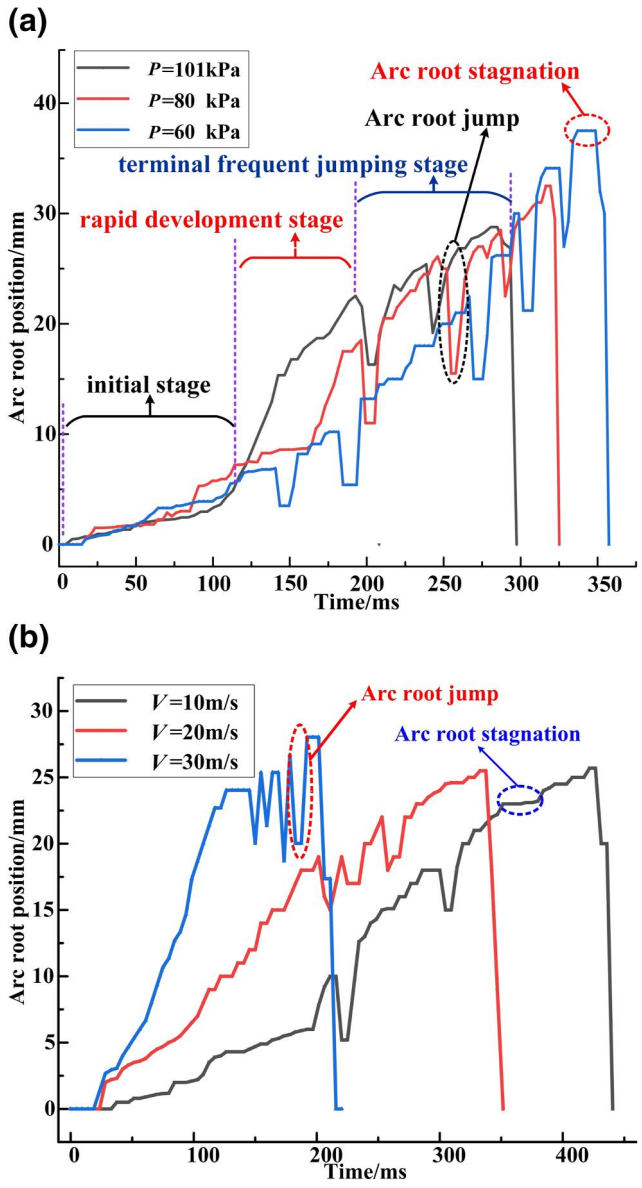

FIGURE 5 Variation of the arc root position of the pantograph-catenary arc with time under different (a) air pressures and (b) airflow velocities

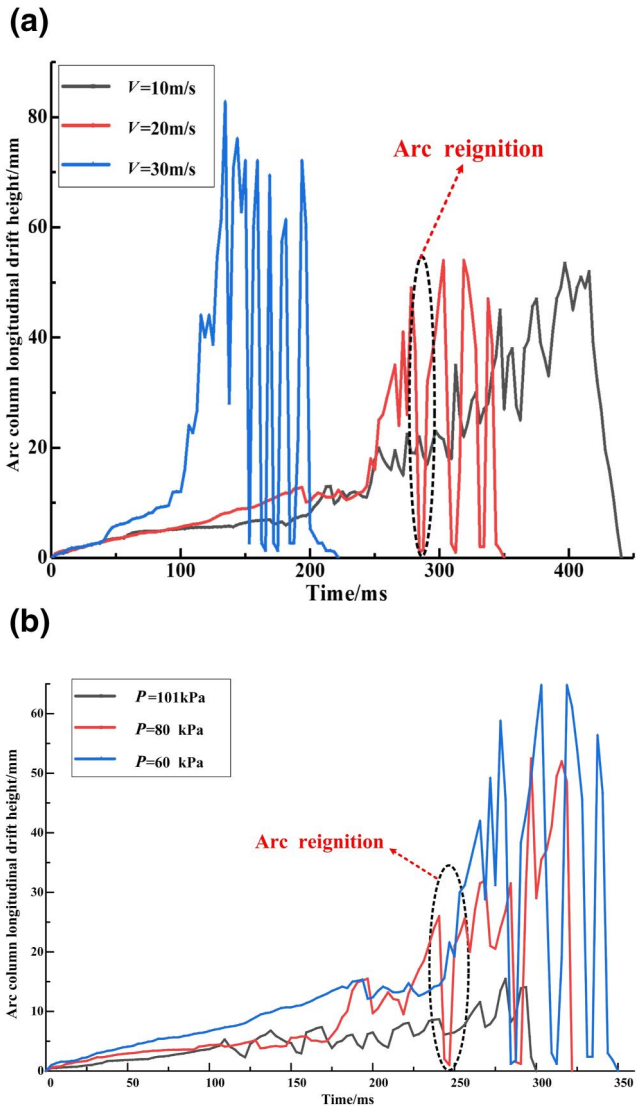

FIGURE 6 The arc column longitudinal drift height varies with time under different (a) airflow velocities and (b) air pressures

current density, and magnetic induction, respectively, and g is the acceleration of gravity.

(4) Electromagnetic field equations:

The arc current density is

$$J = \sigma E \tag{11}$$

$$E = -\nabla\varphi \tag{12}$$

$$\nabla \cdot (\sigma \nabla\varphi) = 0 \tag{13}$$

The arc magnetic field is

$$B = \nabla \times A \tag{14}$$

$$\nabla^2 A = -\mu_v \sigma E \tag{15}$$

E、 and φ are the electric field strength, electric potential, and magnetic vector potential, respectively; μ_v is the vacuum permeability.

The top surface of the contact wire is set as a current density inlet, and the bottom surface of the pantograph strip is regarded as ground. The near-electrode sheath voltage fall between the arc and the electrode is taken into consideration in the pantograph-catenary arc model because the near-electrode sheath voltage fall would affect the energy transfer from the arc to the electrode. The near-electrode sheath on the surface

of the contact wire is represented by a thin layer, whose electrical conductivity is expressed as below [31]:

$$\sigma_e = \frac{\overrightarrow{J}\Delta w_{\text{sheath}}}{U_c} \tag{16}$$

Here, σ_e is the electrical conductivity of the near-electrode sheath. Δw_{sheath} is the thickness of the plasma sheath, whose value is set as 0.1 mm. U_c is the near-electrode sheath voltage fall, the value of U_c is the near-electrode sheath voltage fall, and the value of U_c is 14.5 V in this paper [15, 36]. The near-electrode sheath between the pantograph slide plate and arc is dealt via the LTE-diffusion method, and the thickness of the near-electrode sheath is set as 0.1 mm.

The boundary conditions are set as follows: the carbon skateboard and the catenary are set as anode and cathode, respectively; the lower boundary of the anode is set to ground, and its potential is zero. The input condition of the electric field is set as the current density boundary according to the Neumann boundary condition. The electric field boundary at the bottom of the catenary is based on the Gaussian distribution current density as the current input. The Gaussian current density distribution function is given in Ref. [31]:

$$J = J_{\max} \exp\left(-\beta \cdot \sqrt{x^2 + y^2}\right) \tag{17}$$

J_{max} and β represent the current density and constant at the centre of the cathode spot, respectively; $\sqrt{x^2 + y^2}$ represents the distance between the desired point and the cathode spot. The left and right boundaries of the air domain are set as the inlet and outlet boundary conditions of the airflow, respectively. In addition, the simulation model ignores the moment of arc initiation and sets a high-temperature area between the catenary and the carbon skateboard. The calculation area and the initial temperature of the arc column are set to 300 and 6000 K, respectively.

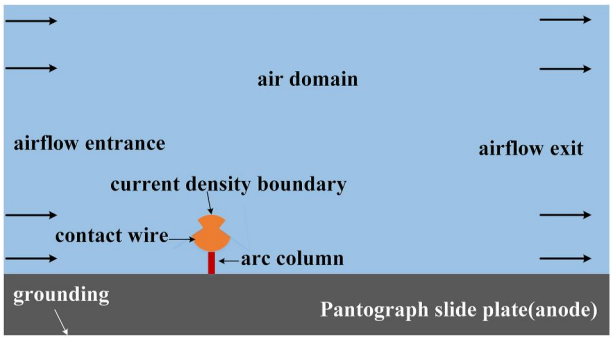

FIGURE 7 Schematic diagram of the geometric model of the pantograph-catenary system

TABLE 1 Physical parameters of the catenary and pantograph contact strip [30, 31]

Physical parameter	Catenary	Pantograph-contact strip
Thermal conductivity (W/(m·K))	398	80
Density (10^3kg/m^3)	9.02	8.1
Specific heat capacity (J/(kg·K))	384	376
Resistivity (μΩ·m)	0.024	0.35

5 | SIMULATION AND ANALYSIS OF THE PANTOGRAPH-CATENARY ARC UNDER LOW AIR PRESSURE AND STRONG AIRFLOW

Based on the above 2-D mathematical model of the pantograph-catenary arc, this study uses the Comsol Multiphysics multi-physics coupling analysis software for calculation and uses the Comsol Multiphysics software's own physics control grid for dissection; the grid contains 5892 elements, the minimum mass is 0.2387, and the average mass is 0.8867. A transient solver is used to calculate the dynamic characteristics of the pantograph arc under different air pressures and airflows. The arc current is set to 100 A, the air pressure is 101, 80, and 60 kPa, respectively, and the airflow is 10, 20, and 30 m/s, respectively. The time step is set to 9.5205 μs.

5.1 | Temperature distribution characteristics of the pantograph-catenary arc under different airflow velocities

To investigate the influence mechanism of air velocity on pantograph-catenary arc movement at the low air pressure, this study simulates the temperature field distribution of the pantograph-catenary arc when the air pressure is 60 kPa and the air velocity is 10, 20, and 30 m/s respectively, as shown in Figure 8.

The airflow velocity has a significant effect on the temperature field distribution of the pantograph-catenary arc. In the initial stage of arc development, the arc develops slowly, and the relative displacement of the arc root movement is about 0 mm. At this stage, the air velocity has almost no effect on the migration movement of the arc root. With the development of the arc, the motion velocity and relative displacement of the arc root at low airflow velocity are lagging. For example, when the airflow velocity is 30 m/s, the arc root moves to a position 18.15 mm from the contact line in 5 ms, and the moving distance of the arc root is 1.84 and 2.87 times when the airflow velocity is 20 and 10 m/s, respectively. This shows that the increase of the airflow velocity can reduce the degree of ablation of the carbon electrode, but the ablation area of the carbon electrode is larger.

In addition, with the increase of airflow velocity, the arc column longitudinal drift is more serious, and the arc column tension is more severe. For example, when the air velocity is 10, 20, and 30 m/s, respectively, the arc column longitudinal drift height is 8.51, 11.01, and 16.12 mm when the pantograph-catenary arc is developed to 5 ms.

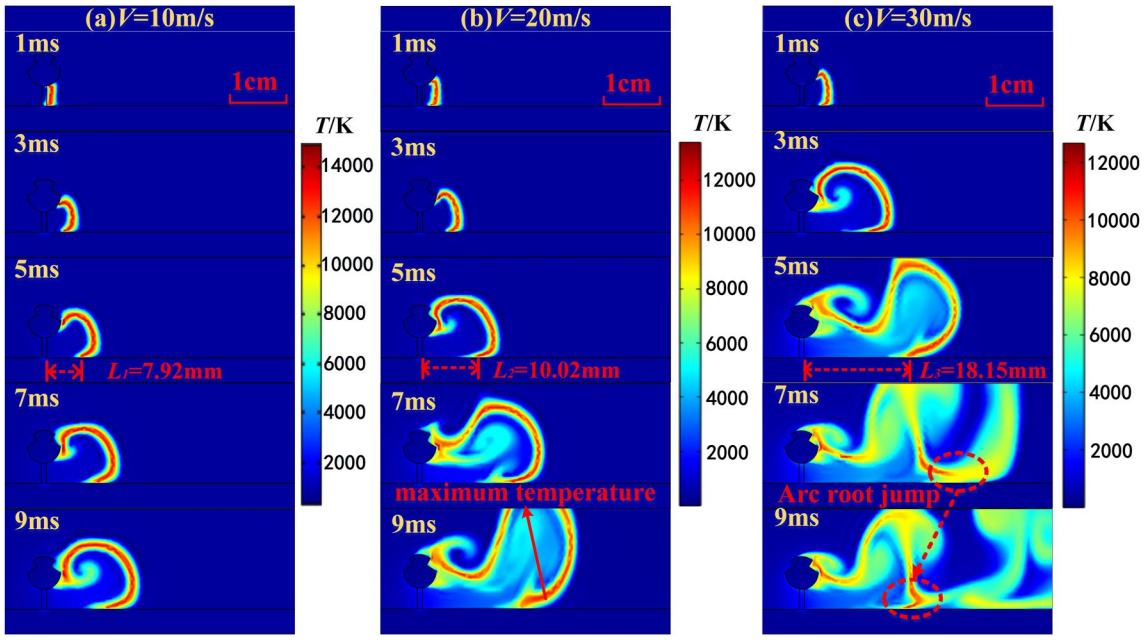

FIGURE 8 The development characteristics of pantograph-catenary arc movement under different airflow speeds

To further investigate the influence of airflow velocity on the arc root movement and the longitudinal drift behaviour of the arc column, the arc root movement velocity and the arc column longitudinal drift velocity in the stable arc burning stage (3–7 ms) are calculated, and the results are shown in Figure 9. When the airflow velocity is 10, 20, and 30 m/s, the arc root movement velocity is 1.59, 2.11, and 3.63 m/s, respectively, and the arc column longitudinal drift velocity is 1.72, 2.21, and 3.22 m/s, respectively, which is also consistent with the experimental results. With the increase of airflow velocity, the longitudinal arc drift velocity and height of the arc column increase, which also shows that the arc is easier to drift to the bus bar under low air pressure and high-speed airflow, which seriously threatens the supporting insulator.

Figure 10a shows the maximum temperature change of the pantograph-catenary arc under different airflow velocities when the air pressure is 60 kPa. It can be seen from the figure that the temperature of the pantograph-catenary arc is significantly negatively correlated with the air velocity. When the air velocity increases from 10 to 30 m/s, the maximum temperature of the pantograph-catenary arc decreases from about 14500 to 13,100 K. In the initial stage of arc development, the maximum temperature of the pantograph-catenary arc has a sharp rise stage and then reaches a relatively stable stage.

It is worth noting that in the stable arc burning stage, the maximum temperature of the pantograph-catenary arc appears to be periodically oscillating at different airflow velocities. The oscillation periods are about 5.52, 2.03, and 1.25 ms, respectively, when the air velocity is 10, 20, and 30 m/s. To further reveal the reason why the temperature oscillation period decreases with the increase of airflow velocity, the arc motion image of the arc network is cut off at the air velocity

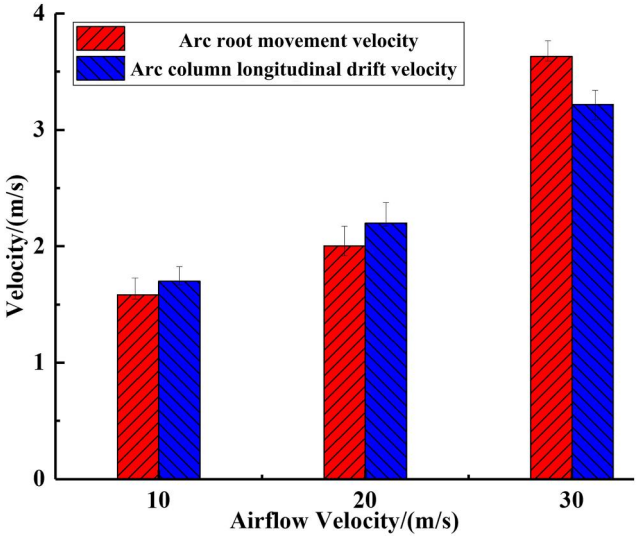

FIGURE 9 Variation of arc root movement velocity and arc column longitudinal drift velocity under different airflow velocities (air pressure is 60 kPa)

of 30 m/s, and it is found that the arc root jump occurs at the highest temperature oscillation of the arc, and the arc temperature drops suddenly during the process of the old arc root transition to the new arc root after the new arc root is formed; The arc channel gradually resumes conduction and the arc temperature increases rapidly; thus an arc temperature oscillation cycle is completed. This also theoretically explains that the arc root jumps more frequently, the stability of arc burning is worse and the arc is easier to extinguish under strong airflow.

It can be seen from Figure 10b that the airflow velocity has a significant effect on the pantograph-catenary arc

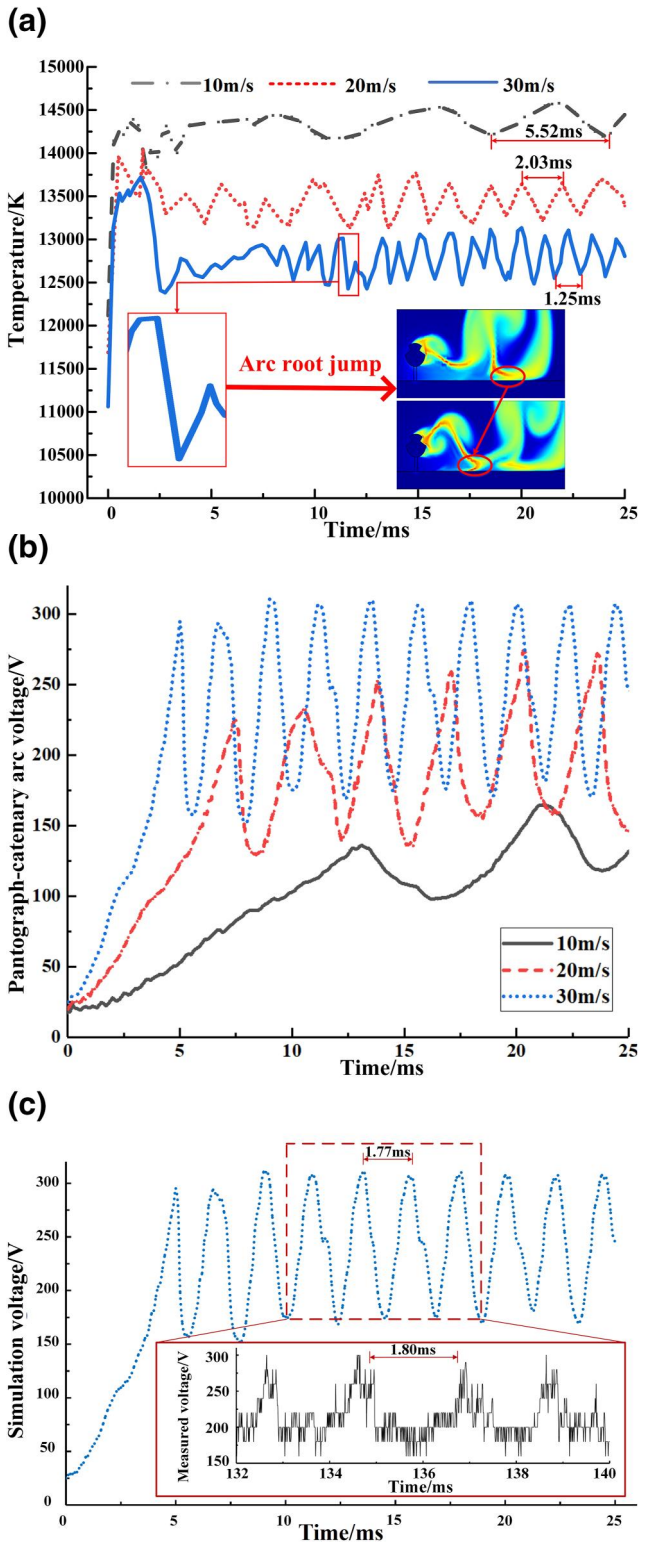

FIGURE 10 Variation curve of (a) pantograph-catenary arc temperature and (b) voltage under different air velocities (air pressure is 60 kPa) and (c) comparison diagram of the experimental voltage waveform and simulation voltage waveform

voltage. When the airflow velocity increases from 10 to 30 m/s, the arc voltage increases from about 150 V to about 300 V. There are two possible reasons for this result: first,

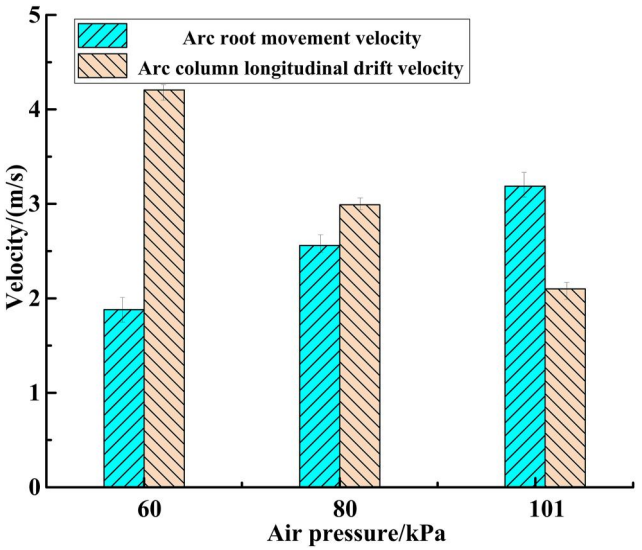

FIGURE 11 Variation of arc root movement velocity and arc column longitudinal drift velocity under different air pressures (airflow velocity is 20 m/s)

with the increase of airflow velocity, the arc column tension intensifies, and the arc voltage increases significantly with the increase of arc column length; second, the convection heat dissipation between the pantograph-catenary arc and air region is accelerated by the influence of airflow, which causes the arc temperature to decrease; thus the resistance and voltage of the arc increases.

Figure 10c is the comparison between the experimental voltage waveform and simulation voltage waveform at the arc ignition stability stage when $P = 60$ kPa and $V = 30$ m/s. It can be seen from the figure that the variation trend of the simulation voltage waveform and experimental voltage waveform is basically the same, and the fluctuation period is 1.77 and 1.80 ms, respectively, based on the ignoring random error in the experiment process. It can be considered that the fluctuation cycle of the two is also consistent. The peak values of both experimental voltage waveform and simulation voltage waveform are about 300 V, which also verifies the accuracy of the simulation.

5.2 | Influence of different air pressures on pantograph-catenary arc motion characteristics

In this study, the arc root movement velocity and the longitudinal arc drift velocity of the arc column in the stable arc burning stage (3–7 ms) under different air pressures are calculated when the airflow velocity is 20 m/s as shown in Figure 11. When the air pressure is 101, 80, and 60 kPa, the arc root movement velocity is 3.19, 2.56, and 1.88 m/s, respectively. At low air pressure, the arc root moves slowly, resulting in a more serious ablation of a carbon electrode and a larger diameter and depth of the ablation pit.

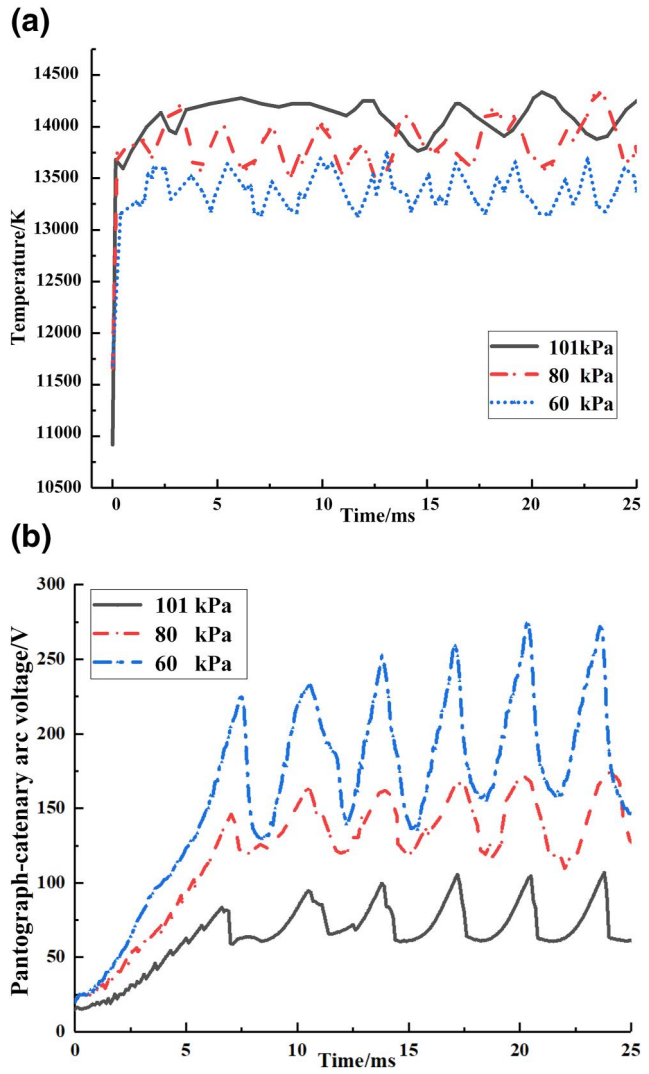

FIGURE 12 Variation curve of (a) pantograph-catenary arc temperature and (b) voltage under different air pressures (airflow velocity is 20 m/s)

Moreover, the arc burning time is longer under low air pressure, which further deepens the ablation degree of the carbon slide plate. When the air pressure is 101, 80, and 60 kPa, respectively, the arc column longitudinal drift velocity is 2.10, 3.01, and 4.20 m/s, respectively, which indicates that the longitudinal arc drift height of the arc column is higher under low air pressure, and it is easier for the arc to move to the catenary bus bar and cause flashover of the supporting insulator.

The curves of maximum temperature and arc voltage of the pantograph-catenary arc under different air pressures are extracted as shown in Figure 12. Generally speaking, the arc temperature at low air pressure is slightly lower than that at high pressure. When the air pressure decreases from 101 to 60 kPa, the maximum temperature of the pantograph-catenary arc decreases from 14100 to 13,800 K. It is worth noting that the maximum temperature of the arc oscillates with different frequencies at different air pressures. With the decrease of air pressure, the oscillation frequency decreases, which is consistent with the conclusion that the arc root jumps more frequently at low air pressure.

It can be seen from Figure 12b that the voltage of the pantograph-catenary arc increases with the decrease of air pressure. When the air pressure decreases from $P = 101$ to 60 kPa, the arc voltage increases from about 105 V to about 270 V. Combined with Figure 11 analysis, it can be seen that under the condition of fixed air velocity, the longitudinal arc drift phenomenon of the arc column of the pantograph-catenary arc column is serious under low pressure, and the length of the arc column is long, which leads to a significant increase of arc column voltage of the pantograph-catenary arc. In addition, the longer arc column leads to the increase of heat loss, the decrease of arc temperature, the increase of arc resistance, and the increase of arc voltage.

6 | CONCLUSION

(1) The traction mechanism of the arc root-arc column movement of the pantograph-catenary arc under low air pressure and strong airflow are summarized. The arc root movement is divided into the initial stage, rapid development stage, andterminal frequent jumping stage. In the initial stage, the arc movement form is the arc root traction arc column, which accounts for about one-third of the total arc burning time. The stagnation duration of the arc root determines the degree of electrode ablation. However, in the rapid development stage and terminal frequent jumping stage, the traction mechanism of arc movement is the arc column traction arc root. In these two stages, the arc movement forms are mainly the longitudinal drift movement and the frequent jump of the arc root.

(2) When the pantograph-catenary system is placed under low air pressure, arc burning duration and arcing root stagnation duration increase dramatically. Arc burning time and arcing root stagnation time at 60 kPa are 1.73 and 2.21 times of those at atmospheric pressure, respectively, which leads to more serious electrode ablation under low air pressure. Along with the air velocity increasing, the arc stability gets worse, meanwhile the arc is easier to extinguish. However, the longitudinal drift velocity and height of arc column are greater; arc burning duration and arc column longitudinal drift velocity when the airflow velocity is 30 m/s is 0.5 and 2.51 times of that when the airflow velocity is 10 m/s, respectively. The longitudinal drift of the arc column is likely to lead to flashover of the supporting insulator.

(3) Two typical irregular arc motion phenomena under low air pressure and strong airflow found during the process of arc burning: arc root jumping and arc reignition. The arc root

jumps more frequently under low air pressure. When the air pressure is 60 kPa, 80 kPa, and 101 kPa, the average number of arc root jumps are 5.2, 2.9, and 1.8, respectively; the arc reignition frequency increases with the increase of airflow velocity when the air pressure is 60 kPa, the airflow velocity is 10, 20, and 30 m/s; meanwhile the arc reignition frequency is 0, 3.1 and 4.2, respectively; the physical explanation of arc root jumps and arc reignition is provided.

(4) The influence of different air pressures and airflow velocities on arc temperature and voltage of the pantograph-catenary arc is calculated. The arc temperature under low air pressure and strong airflow decreases, and the periodic oscillation phenomenon appears. The oscillation period decreases with the increase of the airflow velocity. The arc voltage increases significantly under low air pressure and strong airflow, and the fundamental reason for arc voltage variation is found from arc length, arc diameter, and arc temperature.

ACKNOWLEDGEMENT

Natural Science Foundation, Grant/Award Number: U19A20105, 51807167, 51922090, 52077182, 51837009, SGTYHT/19-JS-215, NEEC-2018-B06

CONFLICT OF INTEREST

None.

DATA AVAILABILITY STATEMENT

Data sharing is not applicable to this article as no data sets were generated or analysed during the current study.

ORCID

Wenfu Wei https://orcid.org/0000-0003-2514-2243
Zefeng Yang https://orcid.org/0000-0002-5893-678X
Wenhan Xie https://orcid.org/0000-0001-7911-979X

REFERENCES

1. Yang, Z., et al.: Thermal characterization of dielectric barrier discharge plasma actuation driven by radio frequency voltage at low pressure. High Volt. 3(2), 154–160 (2018)
2. Sun, J., et al.: Metal particle movement and distribution characteristics under AC voltage and ball-plane electrodes. High Volt. 4(2), 138–143 (2019)
3. Wu, S., et al.: Effect of surface modification of electrodes on charge injection and dielectric characteristics of propylene carbonate. High Volt. 5(1), 15–23 (2020)
4. Ding, T., et al.: Arc erosive characteristics of a carbon strip sliding against a copper contact wire in a high-speed electrified railway. Tribol. Int. 79(11), 8–15 (2014)
5. Midya, S., et al.: Pantograph arcing in electrified railways-mechanism and influence of various parameters-part II: with AC traction power supply. IEEE Trans. Power Deliv. 24(4), 1940–1950 (2009)
6. Wei, W.F., et al.: Influences of pantograph-catenary arc on electrical characteristics of a traction drive system. High Volt. Eng. 44(5), 1589–1597 (2018) (in Chinese)
7. Gao, G.Q., et al.: Dynamics of pantograph-catenary arc during the pantograph lowering process. IEEE Trans. Plasma Sci. 44(11), 2715–2723 (2016)
8. Wu, G.N., et al.: Research advances in electric contact between pantograph and catenary. High Volt. Eng. 42(11), 3495–3506 (2016) (in Chinese)
9. Hejripour, F., et al.: Study of mass transport in cold wire deposition for wire arc additive manufacturing. Int. J. Heat Mass Tran. 125, 471–484 (2018) (in Chinese)
10. Xie, W.H., et al.: Study on the erosion characteristics of copper-carbon electrode pairs by DC air arc. High Volt. 6(4), 674–683 (2021)
11. Yin, J., Wang, Q., Li, X.: Simulation analysis of arc evolution process in multiple parallel contact systems. IEEE Trans. Plasma Sci. 46(8), 2788–2793 (2018)
12. Rong, M.Z., et al.: Review of microscopic property calculation of equilibrium and non- equilibrium arc plasma. Trans. China Electrotech. Soc. 31(19), 54–65 (2016) (in Chinese)
13. Lin, X., Wang, N., Xu, J.Y.: Arcing model of a disconnector and its effect on VFTO. Plasma Sci. Technol. 15(7), 644–647 (2013)
14. Iturregi, A., et al.: Electric arc in low-voltage circuit breakers: experiments and simulation. IEEE Trans. Plasma Sci. 45(1), 113–120 (2017)
15. Yang, F., et al.: Numerical analysis of the influence of splitter-plate erosion on an air arc in the quenching chamber of a low-voltage circuit breaker. J. Phys. D Appl. Phys. 43(43), 434011 (2010)
16. Mao, H., et al.: On-line monitoring of pressure in vacuum interrupters. IEEE Trans. Dielectr. Electr. Insul. 14(1), 179–184 (2007)
17. Chen, Y., et al.: Influence of the axial magnetic field on sheath development after current zero in a vacuum circuit breaker. Plasma Sci. Technol. 19(6), 24–29 (2017)
18. Chang, L.C., Wei, Y.: Reciprocating motion of magnetically driven arcs in air at low critical atmospheric pressure. IEEE Holm Conference on Electrical Contacts. 9, 26–29 (1988)
19. Benilov, M.S., et al.: On the mechanism of retrograde motion of cathode spots of vacuum arcs. ISDEIV. 11(19), 23–28 (2018)
20. Chen, W.J., et al.: Simulation for secondary arc caused by single-phase grounding in UHV AC transmission line. High Volt. Eng. 36(1), 1–6 (2010) (in Chinese)
21. Sun, Q.Q., et al.: Experimental research on secondary arcs of UHV half-wavelength ACT ransmission Lines. High Volt. Eng. 38(2), 350–358 (2012) (in Chinese)
22. Zhang, Z.J., et al.: Propagation of partial arc during the DC pollution flashover process for insulator string at low air pressure. Proc. Chin. Soc. Electr. Eng. 29(25), 104–110 (2009)
23. Guo, F.Y., et al.: Electromagnetic noise of pantograph arc under low current conditions. Int. J. Appl. Electromagn. Mech. 53(3), 397–408 (2017)
24. Gao, G.Q., et al.: Magnetohydrodynamics modeling analysis of arc under lowering pantograph with load condition. High Volt. Eng. 45(12), 3916–3923 (2019) (in Chinese)
25. Hao, J., et al.: Model of coupled pantograph-catenary arc and electrodes considering electrodes melting. High Volt. Eng. 44(5), 1668–1676 (2018) (in Chinese)
26. Wei, W.F., et al.: Study on pantograph arcing in a laboratory simulation system by high-speed photography. IEEE Trans. Plasma Sci. 44(10), 2438–2445 (2016)
27. Liu, X., et al.: Multi-physics analysis and optimization of high-speed train pantograph catenary systems considering velocity skin effect. High Volt. 5(6), 654–661 (2020)
28. Wei, W.F., et al.: Highly conductive graphite matrix/copper composites by a pressureless infiltration method. J. Appl. Phys. 130(1), 015102 (2021) (in Chinese)
29. Yang, Z.F., et al.: Influence of the crosswind on the pantograph arcing dynamics. IEEE Trans. Plasma Sci. 48(8), 2822–2830 (2020)
30. Zhu, G., et al.: Modeling pantograph–catenary arcing. Proc. Inst. Mech. Eng. - Part F J. Rail Rapid Trans. 10(7), 1687–1697 (2015)
31. Xu, P., et al.: Modeling and simulation of arc and contact wire molten pool behavior during pantograph lowering process. AIP Adv. 8(11), 115008 (2018)

32. Murphy, A.B.: Transport coefficients of air, argon-air, nitrogen-air, and oxygen-air plasmas. Plasma Chem. Plasma Process. 15(2), 279–307 (1995)
33. Lowke, J.J.: Predictions of arc temperature profiles using approximate emission coefficients for radiation losses. J. Quant. Spectrosc. Radiat. Transf. 14(2), 111–122 (1974)
34. Naghizadeh-Kashani, Y., Cressault, Y., Gleizes, A.: Net emission coefficient of air thermal plasmas. J. Phys. D Appl. Phys. 35(22), 2925–2934 (2002)
35. Ragaller, K., et al.: Dielectric recovery of an axially blown SF6-Arc after current zero: part II-theoretical investigations. IEEE Trans. Plasma Sci. 10(3), 154–162 (1982)
36. Coulombe, S., Meunier, J.L.: A comparison of electron-emission equations used in arc - cathode interaction calculations. J. Phys. D Appl. Phys. 30(20), 2905–2910 (1997)

How to cite this article: Xu, Z., et al.: Characteristics of pantograph-catenary arc under low air pressure and strong airflow. High Volt. 7(2), 369–381 (2022). https://doi.org/10.1049/hve2.12180